2018

Modeling A Reciprocating Compressor Using A Two-Way Coupled Fluid And Solid Solver With Automatic Grid Generation And Adaptive Mesh Refinement

David Henry Rowinski
Convergent Science, Inc., United States of America, david.rowinski@convergecfd.com

Jasim Sadique
Convergent Science, Inc., United States of America, jasim.sadique@convergecfd.com

Sidnei Jose De Oliveira
Tecumseh Products Co, United States of America, sidnei.oliveira@tecumseh.com

Marcelo Real
Tecumseh Products Co, United States of America, marcelo.real@tecumseh.com

Modeling a Reciprocating Compressor Using a Two-Way Coupled Fluid and Solid Solver with Automatic Grid Generation and Adaptive Mesh Refinement

David ROWINSKI[1]*, Jasim SADIQUE[1], Sidnei OLIVEIRA[2], Marcelo REAL[2]

[1]Convergent Science, Inc.
Madison, WI, USA
608-230-1528
david.rowinski@convergecfd.com

[2]Tecumseh Products Company
Ann Arbor, MI, USA

* Corresponding Author

ABSTRACT

Computational fluid dynamics has been increasingly used in the design and analysis of reciprocating compressors over the last several years. One of the major challenges in the use of such tools is the creation of the numerical grid on which the modeled equations are solved. Since these compressors typically consist of many interconnected and moving parts, manual creation of the grid can be labor-intensive. Furthermore, it is necessary that the choice of grid yields a sufficiently resolved solution, so that the numerical error is significantly less than the modeling error. In this work, a small displacement refrigeration compressor is modeled using a numerical grid created with an automatic meshing approach. The grid is then automatically adapted to the flow based on the local flow field variables at each time step. This cut-cell based grid matches the supplied fluid volume exactly and permits general motion of all bounding surfaces. An explicit two-way coupled approach is used to account for the fluid-structure interaction between the deforming reed valves and the flow. The fluid is solved using a finite-volume approach, whereas the solid is solved using a finite-element model. The model is validated in comparison to measured mass flow rate, pressure, temperature, and valve lift for two different operation conditions and two different working fluids, namely R-404a and R-449a. The numerical accuracy of the calculations is demonstrated through an automated grid convergence study, and the effect of the grid and time-step resolution on the pressure pulsations and valve lift is shown. While computations on a relatively coarse grid yield power, mass flow rate, and pressure oscillation frequency comparable to measurements, a finer mesh is required inside the cylinder and in the discharge muffler to predict adequately the amplitude of the pressure fluctuations.

1. INTRODUCTION

As regulations on refrigeration compressors continue to tighten all across the world, it is more and more important for designers to understand the flow in the devices they develop. While there are many methods for modeling the flow in such devices, three-dimensional computational fluid dynamics (CFD) has some distinct advantages, most importantly giving designers access to the time-varying flow fields in three dimensional space and how it is affected by the exact design geometry. Other advantages include the identification of flow structures important to viscous losses, local heat transfer, and mixing. These models are more complete than reduced order models in the sense that they are mostly free from empirical corrections which make them applicable over wider ranges of operating conditions or geometry variations. As Prasad (2004) points out in his review, though reciprocating compressors are typically viewed as thermodynamic devices, most of the important losses are fluid dynamic in nature, making understand the flow of critical importance.

Researchers have made considerable advancement in the application of CFD models to reciprocating compressors over the last twenty-five years. Cyklis (1994) applied a commercial CFD package to model two-dimensional flow

through a suction valve. Fagotti and Possamai (2000) applied commercial CFD tools to model flows in compressor components, and noted that one important aspect of the problem setup was the user selection of grid size. Ottitsch (2000) applied CFD to model a variety of different valve types in steady state incompressible flow. Chikurde (2002) presented an analysis of a full compressor geometry and noted that it was critical to apply sufficient grid resolution in regions of important flow features. In addition, complex flow features such as rivets and fillets were removed to simplified the meshing procedure. More recently, Kim (2006) applied two-way coupled fluid-structure interaction (FSI) to model the behavior of valves, and Pereira (2007) applied CFD to model the full three-dimensional domain of a refrigeration compressor. Pereira (2008) compared models of various levels of complexity and found advantage of the CFD's predictive nature, despite finding the three-dimensional model costs too high for use in optimization. Mistry (2012) and Rigola (2012) explored three-dimensional modeling of the flow over valves, among other topics such as turbulence model effects. Rodrigues (2014) applied a variety of turbulence models to full three-dimensional compressor models.

All of the aforementioned CFD studies of reciprocating compressors required the users to construct a numerical mesh on which the governing equations are solved. As pointed out by Prasad (2004) and others, this grid generation process is a major bottleneck in the routine application of CFD for design purposes. Furthermore, it is essential to show that the numerical error in the solution of the discretized governing equations is small compared to the modeling error in order for the models to be evaluated correctly. Several more recent studies, including Rowinski (2016) and Silva (2017), applied automated meshing procedures in which this bottleneck step is removed.

In the present study, the same automated meshing approach as Rowinski (2016) and Silva (2017) is applied to a different type of reciprocating compressor. A new model for treating the motion of the reed valves is introduced, and the numerical error in the simulations is quantified through an automated grid convergence study. The results are compared to the previous studies with similar meshing methodologies to help establish more universal guidelines on automated mesh creation settings that yield numerically accurate results.

2. TEST CASE DESCRIPTION

The compressor to be analyzed in this work is a small refrigeration compressor with a displacement of approximately 16 cubic centimeters. The next sections describe in more detail the geometry of the compressor, whose gas flow path is depicted in Figure 1, the test conditions, and the measurements conducted.

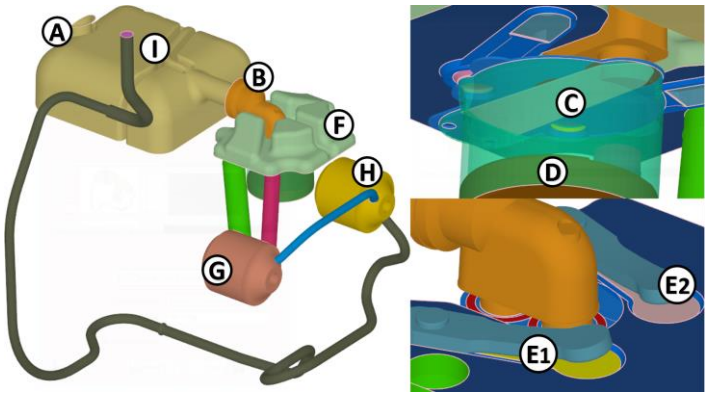

Figure 1: Pictured on the left is the gas flow path in the compressor studied. On the top right is a close-up view of the suction valve. On the bottom right is a close-up view of the discharge valves.

2.1 Geometry

The gas flow path of the compressor, as shown in Figure 1, begins at the suction muffler inlet (A). The gas then travels through the suction muffler, and into the suction port (B). From there it passes through the suction reed valve (C), and enters the cylinder. The cylinder volume is expanded and compressed through the piston (D). The compressed gas leaves the cylinder through the pair of discharge reed valves (E1) and (E2), and enters the discharge chamber (F). The compressed gas then passes through the first discharge muffler (G), and then the second discharge muffler (H), and travels through the discharge line until it exits the discharge line outlet (I).

2.2 Operating Conditions

The compressor was originally designed for use with refrigerant R-404a as the working fluid. R-404a has the desirable property of zero ozone depletion potential (ODP), however it has a relatively large global warning potential (GWP) of 3922. An alternative refrigerant being researched as a replacement is R-449a, which has not only zero ODP, but also a much lower GWP of 1282, approximately a third that of R-404a, as described by Pansulla (2016). Table 1 compares the specifications of both fluids.

Table 1: Properties of the two working fluids examined in this compressor.

		R-404a		**R-449a**	
Mass Percent	R-32	--		24.3%	
	R-125	44%		24.7%	
	R-134a	4%		25.7%	
	R-143a	52%		--	
	R-1234yf	--		25.3%	
Molecular Weight		97.6 g/mol		87.2 g/mol	
ODP		0		0	
GWP		3922		1282	
Tested Conditions		ASHRAE	ARI	ASHRAE	ARI

For each working fluid, two different operating conditions are examined. The first load condition is from an American Society of Heating, Refrigeration, and Air-Conditioning (ASHRAE) standard, and the second is from an Air-Conditioning and Refrigeration Institute (ARI) standard. The ASHRAE condition has a larger superheat and mass flow rate about 70% lower for both working fluids. Compared to R-404a conditions, the R-449a conditions have a lower mass flow rate about 60% lower. In all the tests, the compressor operates at a frequency of 60 Hz.

2.3 Measurements

For each of the four test conditions, a multitude of measurements are recorded from the compressor. This includes pressure measurements at six locations: suction muffler inlet, suction chamber (Figure 2c), cylinder head (Figure 2c), first discharge muffler, and second discharge muffler). Gas temperature measurements are made at six similar locations as well as in the ambient inside the compressor shell. Wall temperatures measurements are taken at the suction muffler, cylinder head, discharge mufflers, and through several of the other mechanical components not

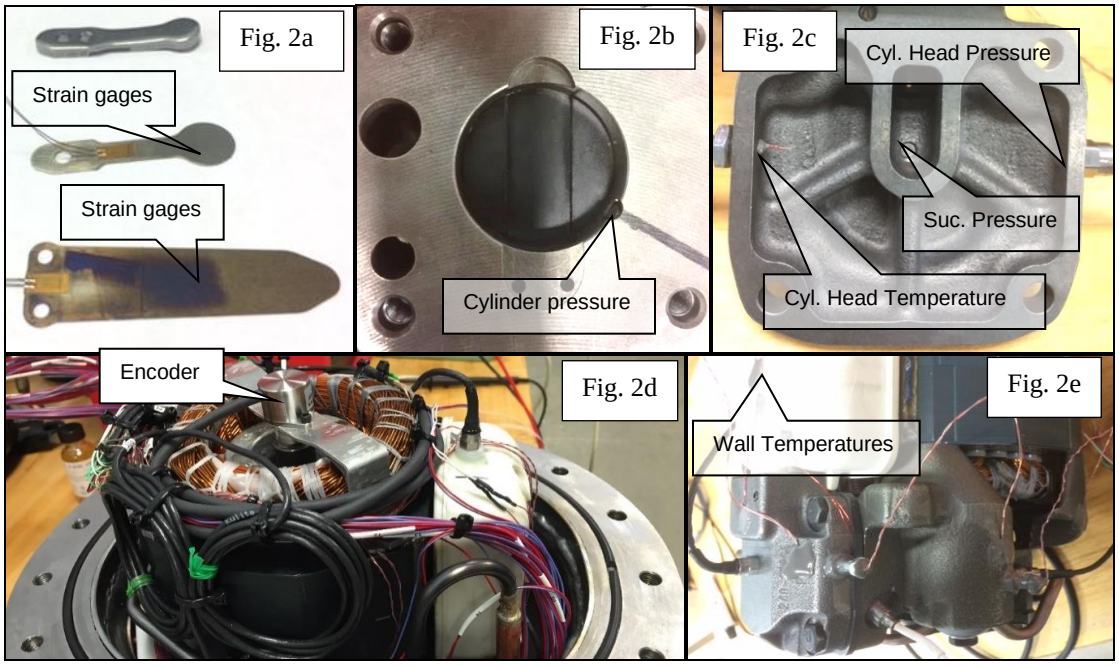

Figure 2. Pictures of the experimental test compressor setup and measurement locations.

directly in contact with the flow path considered in this analysis (Figure 2e). The deflections of the suction and discharge valves are measured using strain gauges bonded to each valve (Figure 2a). The deflection at the center of each valve port is determined from a calibration of each strain gauge sensor. All sensors were synchronized with the crankshaft angular position. An encoder was coupled at the shaft and the top dead center was used as a zero reference (Figure 2d).

3. METHODOLOGY

In order to model the flow in the compressor described above, a numerical method similar to that in Rowinski (2016) and Silva (2017) is employed. The Cartesian cut-cell based method developed in Senecal (2007) and Richards (2017) in the commercially available package, CONVERGE, begins from a triangulated surface which describes the volume of a computational domain. Figure 1 depicts this bounding surface of the domain in this study. The volume is filled by an orthogonal base grid of a user-specified size. Wherever the triangulated surface intersects the base grid, the base grid cells are cut into arbitrary sided polyhedra. Thus the volume represented in the cut-cells is exactly the same as the volume of the original triangulated surface, independent of the base grid size used. Because the process of forming the mesh is entirely automatic, it can easily accommodate complex boundary shapes and complex boundary motion without any user intervention. Because the method is based on standard orthogonal grids, it is computationally simple and exhibits high numerical stability.

3.1 Flow Solver

The conservation equations for mass, momentum, and turbulence quantities are solved using the finite-volume method. All values in the model are collocated at the center of the computational cells. The algorithm of Rhie and Chow (1983) is used to prevent checker-boarding in the velocity and pressure fields. In the present study, second-order spatial discretization is used for solving all the conservation equations. To maintain stability, a fully implicit first-order scheme for time discretization is used in this work. The transport equations are solved using a modified Pressure Implicit with Splitting of Operators (PISO) method from Issa (1985) and successive over-relaxation (SOR) iterative method. A variable time-step approach is used to ensure stability and to increase the time step when possible. The time step is controlled through the Courant-Friedrichs-Lewy (CFL) numbers based on local cell sizes, velocity, speed of sound, and diffusivity.

It is essential to ensure that the grid resolution at any location is sufficiently small to have minimal impact on the solution of the flow field. In most cases, it is very difficult to determine beforehand the locations and times over which a finer grid resolution is required. Automatic Mesh Refinement (AMR) is employed in these models to provide a way to handle this problem. Ideally, a good AMR method should add the cells where the simulation is most under-resolved, or where the sub-grid scale variation of a field variable is the largest. As shown by Pomraning (2000) and others, the refinement criteria is based on the instantaneous curvature of the solution fields.

3.2 Solid Solver and Coupling to Flow Solver

A very important component of the model to simulate accurately is the deflection of the reed valves. As opposed to the previous works of Rowinski (2016) which used a finite-volume formulation of an Euler-Bernoulli cantilever beam, a revised finite-element formulation is used here. As shown in Figure 3, the beam is divided into elements along its length which have two degrees of freedom, namely rotation and deflection. The mass, stiffness, and

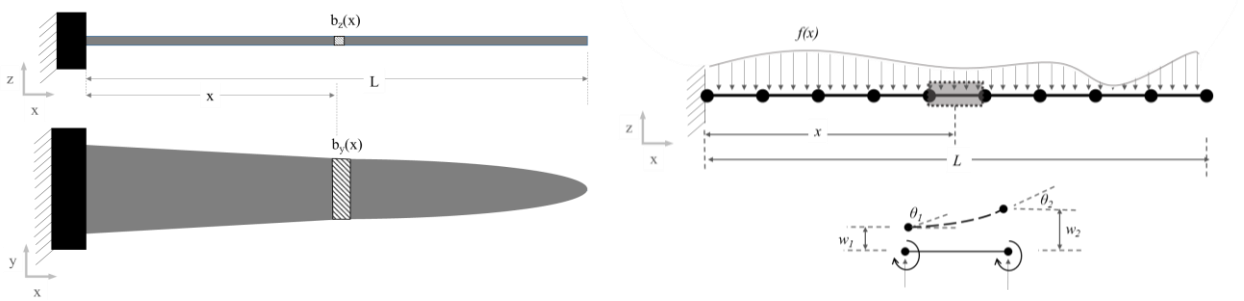

Figure 3: Illustration of the model used for the reed valves. To the left is an illustration of (top) the beam in the length-wise and height-wise view plane, and (bottom) the length-wise and span-wise view plane. To the right is a cross section which depicts how the varying load across the length of the beam is applied to the finite elements.

damping matrices and force vector form a second-order linear system. The time advancement scheme used is the Hilber-Hughes-Taylor (HHT-α) method of Hilber (1977). The model can handle contact of the beam with rigid bodies whereby a penalty penetration model imposes the contact condition between the beam and the rigid body.

The fluid and solid domains are coupled in an explicit manner. At a given time step, the pressure and viscous forces on the beam are calculated after the flow is computed and transferred to the beam model. This force is used to compute the deflections, which are then transferred back to the fluid domain to move the beam boundaries at the next time step. To calculate the force on the beam, a uniform force is assumed to act on each beam element. This uniform force is calculated by identifying the surface triangles connected to each element and calculating the average pressure and viscous force.

3.3 Models and Solution Strategy

A compressible gas formulation is used for the fluid in the model. A structured two-dimensional lookup table with bi-linear interpolation is used to compute the density given the temperature and pressure instead of a conventional equation of state. A reverse lookup function computes the temperature given the pressure and internal energy. The molecular viscosity and conductivity are evaluated in the same way. For both fluids, the CoolProp library from Bell (2014) is used to construct the property tables. The properties of R-404a come from a mixture equation of state from Lemmon (2003), the viscosity and conductivity are from Geller (2000) and Geller (2001). For R-449a, the properties come from mixture-averaged properties of the components.

Table 2: Components along the gas flow path of the compressor studied and labeled as shown in Figure 1 and associated boundary condition in the CFD model.

Symbol	Component	Momentum Boundary Condition
A	Suction muffler inlet	Inflow, imposed time-varying pressure from measurements
B	Suction port	Stationary, Law-of-the-wall
C	Suction reed valve	Deforming through beam model, Law-of-the-wall
D	Piston	Motion through crank-slider mechanism at measured frequency
E1, E2	Discharge reed valves	Deforming through beam model, Law-of-the-wall
F	Discharge chamber	Stationary, Law-of-the-wall
G, H	Discharge mufflers	Stationary, Law-of-the-wall
I	Discharge line outlet	Outflow, imposed constant pressure from measurements

The boundary conditions at each location from Figure 1 are shown in Table 2. For thermal boundary conditions, a law-of-the-wall model is used together with the measured value for the wall temperature. Simulations are run on a coarse grid for ten cycles to stabilize the temperature in the discharge line. From there, three to five cycles are run on finer grids, beginning from a time shortly after suction valve closure.

4. RESULTS AND DISCUSSION

This section presents and discusses the results of the models described in Section 3 applied to the physical compressor described in Section 2. In all presented results, the pressure, temperature, and valve lifts are normalized. The normalized pressure is defined as $(P-P_s)/(P_d-P_s)$ where P is the pressure, P_s is the suction pressure, and P_d is the discharge pressure. Similarly, the temperature, T, is normalized as $(T-T_s)/(T_d-T_s)$ where T_s is the suction temperature, and T_d is the adiabatic discharge temperature. The valve lift is normalized by the maximum valve lift for each valve.

4.1 Base Case Results

Figure 4 shows the comparison of measured and model pressure in the cylinder for all four test conditions. In order to match the compression and expansion portions of the cycle two changes were made from the nominal model. First, the clearance height was increased by about 0.1 mm. Whether the difference could be attributed to manufacturing tolerances or load-induced deformation of the crankshaft, pins, or connecting rod is not currently known, but is outside the scope of the present work. Secondly, a leakage model is applied in the crevice between the cylinder bore and the piston using an orifice flow equation. These two changes can lead to a large difference in the computed flow rates (reduced between 10-20%) and are certainly worth further investigation. Due to the spatial variation in the cylinder pressure at various points in the cycle, it was crucial to keep the numerical measurement

probe as close as possible to the experimental transducer face and to keep the geometry consistent with the test bench compressor. With these changes made, the model achieves very good agreement to the measured data for the compression and expansion processes. During the discharge valve opening, the behavior of the pressure trace is very

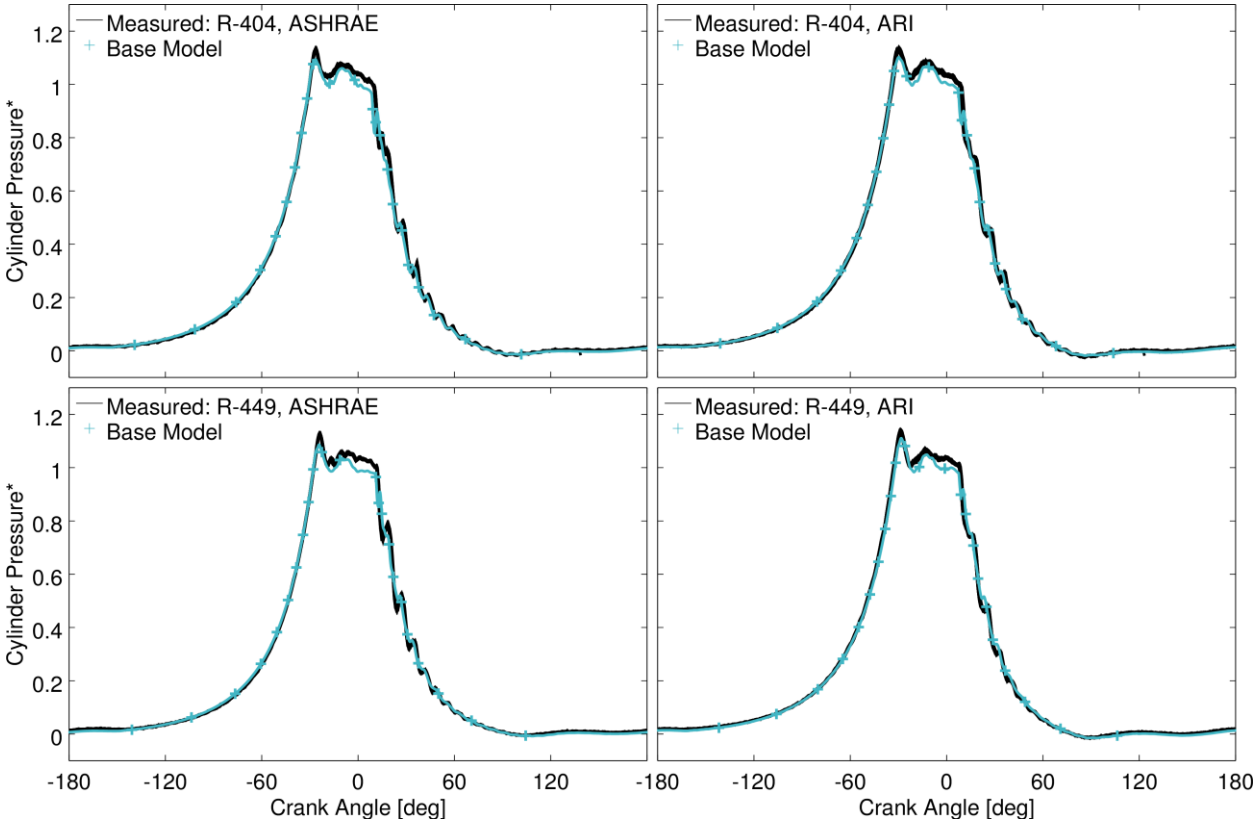

Figure 4: Comparison of measured (solid black line) and modeled (light blue line with cross symbols) pressure in the cylinder for the four different operating conditions.

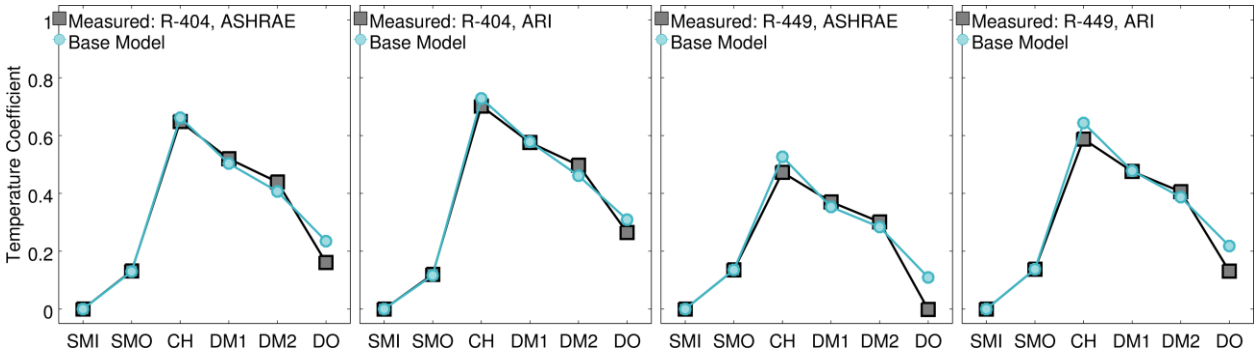

Figure 5: Comparison of measured (black squares) and modeled (light blue circles) temperatures for the four operating conditions, from left to right. Temperatures for each case are shown, from left to right, from the suction muffler inlet, suction muffler outlet, cylinder head, first discharge muffler, second discharge muffler, and discharge outlet.

similar in both measurement and model, however the model consistently under-predicts the magnitude by 2-5% for all four operating points. The model yields a similar behavior in the pressure waves in the cylinder during expansion, with a good prediction of the frequency. Although for some points the magnitude is lower than measured, and at some points the phasing is slightly off.

The average temperature profiles along the flow path are shown in Figure 5. All simulations match the preheat at the suction muffler outlet well, while slightly overpredicting the temperature in the cylinder head for R-449a. The temperature at the discharge outlet is slightly high due to the use of a constant wall temperature boundary condition.

Figure 6 shows the comparison of the measured and modeled valve lifts for the two operating points with R-449a. As with many other modeling studies, the accurate prediction of the expansion and compression are essential to yield an accurate opening profile for each valve. The evolution of the deflection at the port center agreed well between the CFD model with cantilever beams and the measurements, including both the contact of the suction reed with the stopper (evident by the multiple openings), and the contact of the discharge reed with the stopper.

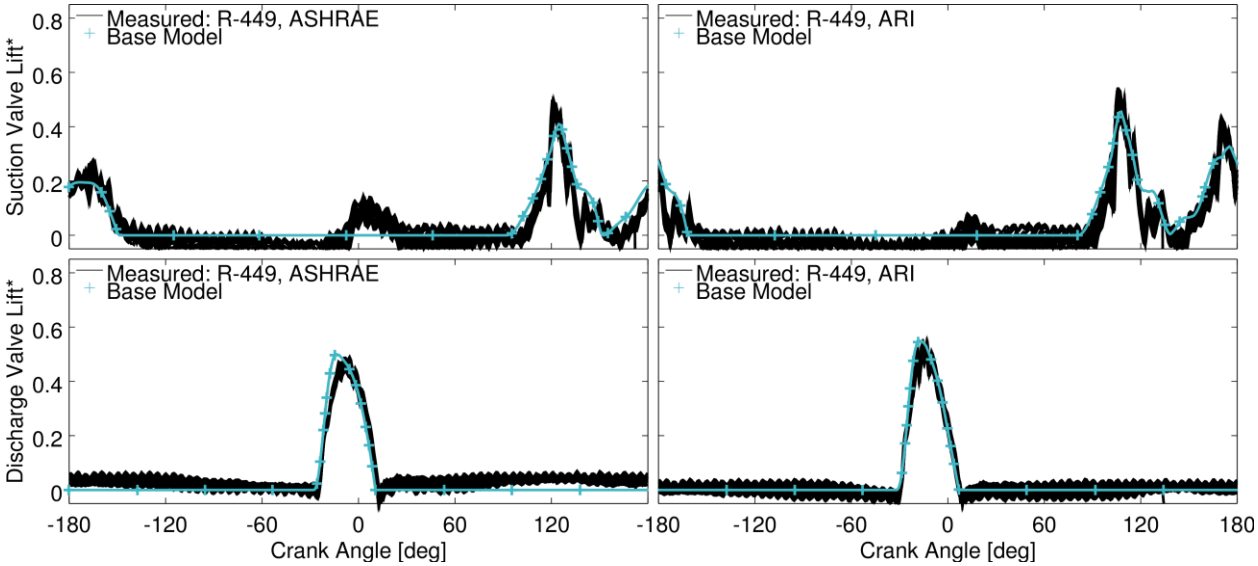

Figure 6: Comparison of measured (black line) and modeled (light blue line with cross symbols) valve lift. The top row shows the suction valve lift and the bottom row shows the discharge valve lift. The columns are divided into two of the tested operating points: ASHRAE condition on the left, and ARI condition on the right.

4.2 Sensitivities to Numerical Parameters

In the use of numerical models where governing equations are discretized in both space and time, it is very important to show that the resolution in both space and time are sufficiently high. For this study, and automated grid convergence study is performed by changing a single parameter, the base grid size. This ensures that the grid is refined proportionally everywhere. Since the time step is controlled by both CFL from local velocity and speed of sound, as the grid is refined the time step is also refined. Representative cut-planes through the suction valve centerline are shown in Figure 7 for four of the grids investigated. More detailed info about each grid is shown in Table 3.

Table 3: Parameters for automated grid creation for four of the grids used in the grid convergence assessment.

	Units	Grid 1	Grid 2	Grid 3	Grid 4
Base grid cells over bore	--	10	20	40	80
AMR scale	--	3	3	3	3
Smallest full cell size	mm	0.40	0.20	0.10	0.05
Minimum cell count	millions	0.05	0.16	0.80	3.2
Maximum cell count	millions	0.18	0.70	3.0	6.0
Number of cores	--	4	8	16	16
Wall clock time	hours/cycle	2.5	6	18	94
Average time step	degrees/time-step	0.109	0.068	0.034	0.015

The results of the grid convergence study are summarized in Figure 8, which shows the pressure at several locations in the domain. For most locations, all grids except Grid 1 (the coarsest grid) provide an adequate prediction of the

pressure evolution in time. The first discharge muffler is the most sensitive to the grid resolution, suggesting that this is a good place for further mesh refinement as also pointed out by Oliveira (2014).

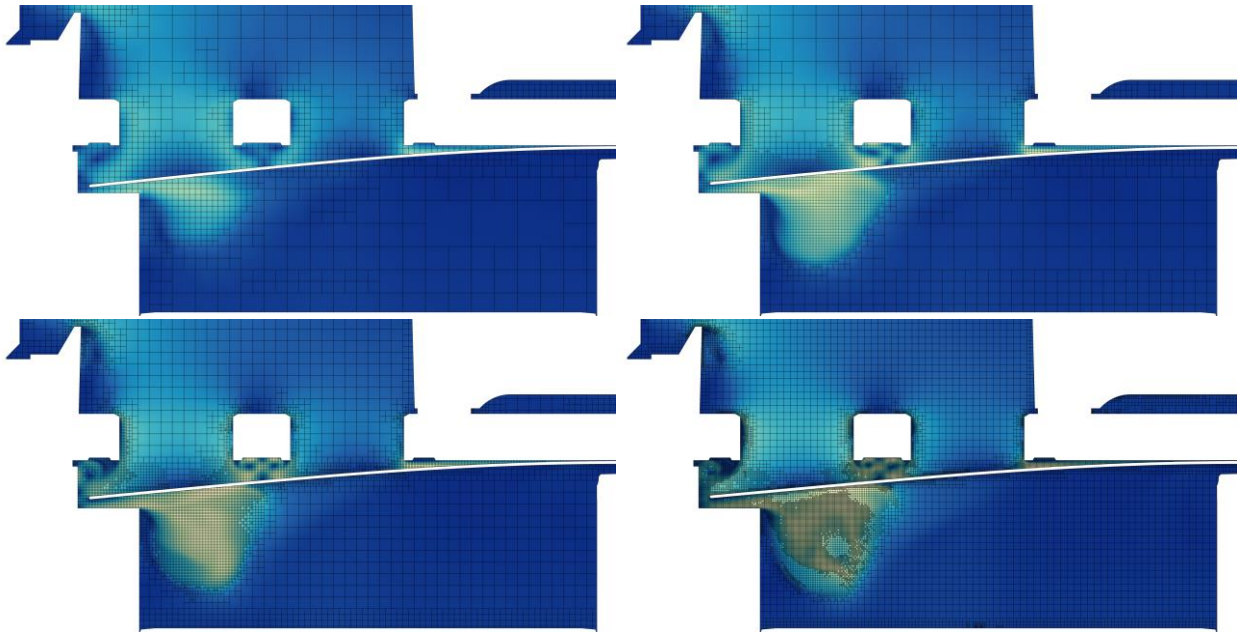

Figure 7: Planes along the suction valve centerline colored by normalized velocity for four of the grids studied in the grid convergence assessment. From left to right are grids 1 and 2 (top row) and grids 3 and 4 (bottom row).

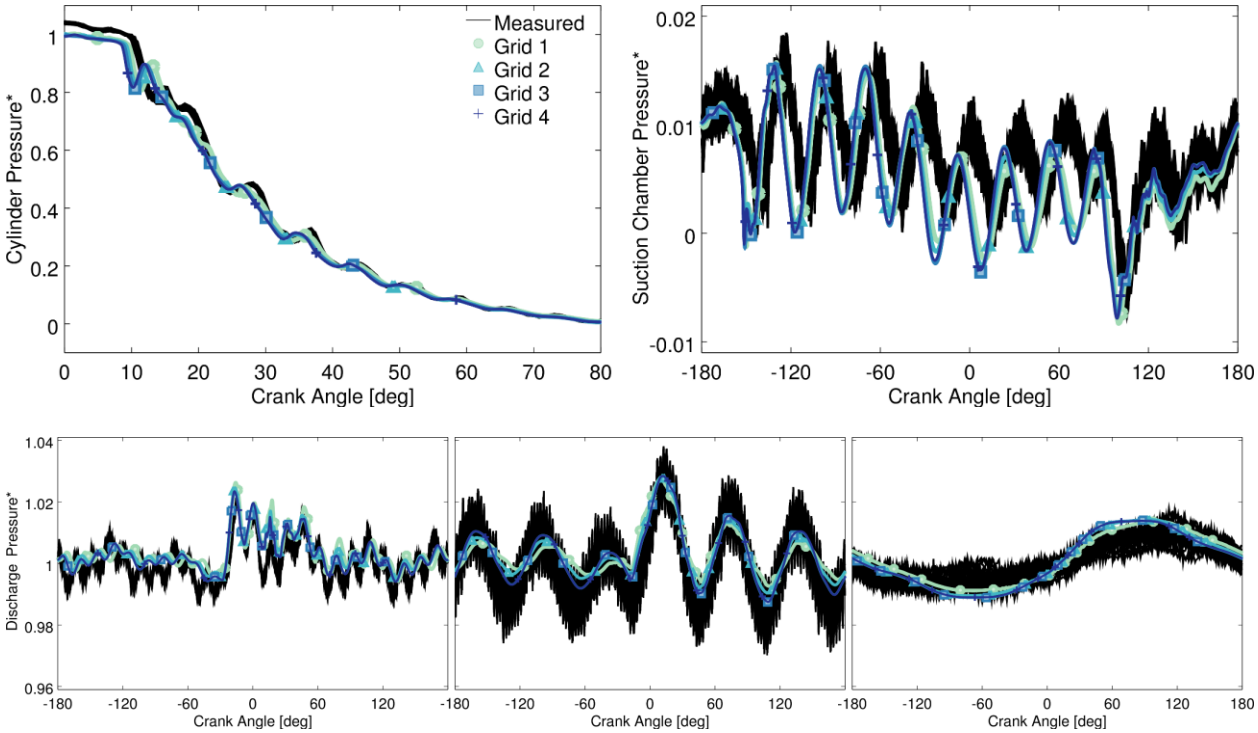

Figure 8: Comparison of measured and modeled pressure at five locations for the R-404a ASHRAE test condition. The black lines are from the measurements, and the modeled results are shown in light green circles (Grid 1), green-blue triangles (Grid 2), blue squares (Grid 3), and dark blue crosses (Grid 4). The top row shows the pressure in the cylinder during expansion (left) and suction chamber (right). The bottom row shows the pressure in the discharge chamber (left), first discharge muffler (center), and second discharge muffler (right).

5. CONCLUSIONS

This work validated a model of a reciprocating compressor at four different operating conditions using automatic grid generation. The results of the model indicate that pressure fluctuations in the cylinder and discharge can be accurately predicted when using an appropriately refined mesh. The results showed that the grid discretization is more important than the temporal discretization when running with a time step limited by both the speed of sound and local fluid velocity. Room for improvement exists in the predictive capability of the beam model, the leakage models, and the thermal boundary conditions particularly along the discharge flow path. A further future goal in this type of application is the use of higher-order numerical schemes which could potentially achieve even better resolution of the pressure waves without requiring such a fine mesh.

REFERENCES

Bell, I.H., Wronski, J., Quoilin, S., Lemort, V. (2014). Pure and Psuedo-pure Fluid Thermophysical Property Evaluation and the Open-Source Thermophysical Property Library CoolProp. *Industrial & Engineering Chemistry Research*, 53 (6), (pp. 2498-2508).

Chikurde, R. C., Loganathan, E., Dandekar, D. P., Manivasagam, S. (2002). Thermal Mapping of Hermetically Sealed Compressors Using Computational Fluid Dynamics Technique. *Proceedings of the 16th International Compressor Engineering Conference at Purdue* (Paper 1520). West Lafayette, USA: Purdue University.

Cyklis, P. (1994). CFD Simulation of the Flow through Reciprocating Compressor Self-acting Valves. *Proceedings of the 12th International Compressor Engineering Conference at Purdue* (Paper 1016). West Lafayette, USA: Purdue University.

Fagotti, F., Possamai, F. C. (2000). Using Computational Fluid Dynamics as a Compressor Design Tool. *Proceedings of the 15th International Compressor Engineering Conference at Purdue* (Paper 1377). West Lafayette, USA: Purdue University.

Geller, V.Z. (2000). Viscosity of Mixed Refrigerants R404A, R407C, R410A, and R507A. *Proceedings of the 8th International Refrigeration Conference at Purdue University* (Paper 508). West Lafayette, USA: Purdue University.

Geller, V.Z., Nemzer, B.Z., Cheremnykh, U.V. (2001). Thermal Conductivity of the Refrigerant mixtures R404A, R407C, R410A, and R507A. *Int. J. Thermophys*., 22 (pp. 1034–1043).

Hilber, H. M., Hughes, T. J. R., Taylor, R. L. (1977). Improved numerical dissipation for time integration algorithms in structural dynamics. *Earthquake Eng. and Struct. Dynamics*, 5 (pp. 283-292).

Issa, R. I, (1985). Solution of the Implicitly Discretised Fluid Flow Equations by Operator-Splitting. *Journal of Computational Physics*, 62.

Karypis, G. (2013). A Software Package for Partitioning Unstructured Graphs, Partitioning Meshes and Computing Fill-Reducing Orderings of Sparse Matrices.

Kim, J., Wang, S., Park, S., Ryu, K., La, J. (2006). Valve Dynamic Analysis of a Hermetic Reciprocating Compressor. *Proceedings of the 18th International Compressor Engineering Conference at Purdue* (Paper 1805). West Lafayette, USA: Purdue University.

Lemmon, E.W. (2003). Pseudo-Pure Fluid Equations of State for the Refrigerant Blends R-410A, R-404A, R-507A, and R-407C. *Int. J. Thermophys*., 24 (4), (pp. 991-1006).

Mistry, H., Bhakta, A., Dhar, S., Bahadur, V., Dey, S. (2012). Capturing Valve Dynamics in Reciprocating Compressors through Computational Fluid Dynamics. *Proceedings of the 21st International Compressor Engineering Conference at Purdue* (Paper 1210). West Lafayette, USA: Purdue University.

Oliveira, S. J., Real, M., Marsh, D. (2014). Simulation of a Refrigeration Compressor Evaluating Accuracy of Results with Variation in 3D Component Discretization. *Proceedings of the 22nd International Compressor Engineering Conference at Purdue* (Paper 2274). West Lafayette, USA: Purdue University.

Ottitsch, F. (2000). CFD: A Viable Engineering Tool for Compressor Valve Design or Just a Toy? *Proceedings of the 15th International Compressor Engineering Conference at Purdue* (Paper 1417). West Lafayette, USA: Purdue University.

Pansulla, A., Allgood, C. (2016). Multi-Year Evaluation of R-449A as a Replacement for R-22 in Low Temperature and Medium Temperature Refrigeration Applications. *International Refrigeration and Air Conditioning Conference at Purdue* (Paper 1761). West Lafayette, USA: Purdue University.

Pereira, E.L.P, Deschamps, C.J., Ribas Jr., F.A. (2007). Performance analysis of reciprocating compressor through CFD simulation. *Proceedings of the International Conference on Compressors and their Systems* (pp. 310-318). London, England: City University of London.

Pereira, E.L.P, Deschamps, C.J., Ribas Jr., F.A. (2008). A comparative analysis of numerical simulation approaches for reciprocating compressor. *Proceedings of the 19th International Compressor Engineering Conference at Purdue* (Paper 1303). West Lafayette, USA: Purdue University.

Pomraning, E. (2000). Development of Large Eddy Simulation Models. *Ph.D. Dissertation, The University of Wisconsin-Madison*.

Pomraning, E., Richards, K., and Senecal, P. (2014). Modeling Turbulent Combustion Using a RANS Model, Detailed Chemistry, and Adaptive Mesh Refinement. *SAE Technical Paper* 2014-01-1116.

Prasad, B. G. (2004). CFD for Positive Displacement Compressors. *Proceedings of the 17th International Compressor Engineering Conference at Purdue* (Paper 1689). West Lafayette, USA: Purdue University.

Rhie, C. M. and Chow, W. L. (1983). Numerical Study of the Turbulent Flow Past an Airfoil with Trailing Edge Separation. *AIAA J*., 21, (pp. 1525-1532).

Richards, K. J., Senecal, P. K., Pomraning, E. (2017). CONVERGE 2.4 Manual, Convergent Science, Madison, WI.

Rigola, J., Lehmkuhl, O., Ventosa, J., Pérez-Segarra, C.D., Oliva, A. (2012). Numerical simulation of the turbulent fluid flow through valves based on Low Mach models. *Proceedings of the 21st International Compressor Engineering Conference at Purdue* (Paper 1375). West Lafayette, USA: Purdue University.

Rodrigues, T. T., Da Silva, D. L. (2014). Turbulence Modelling Evaluation for Reciprocating Compressor Simulation. *Proceedings of the 22nd International Compressor Engineering Conference at Purdue* (Paper 2297). West Lafayette, USA: Purdue University.

Senecal, P. K., Pomraning, E., Richards, K. J., Briggs, T. E., Choi, C. Y., McDavid, R. M., Patterson, M. A., Hou, S., & Shethaji, T. (2007). A New Parallel Cut-Cell Cartesian CFD Code for Rapid Grid Generation Applied to In-Cylinder Diesel Engine Simulations. *SAE Technical Paper*, #2007-01-0159.

Silva, L. R., Dutra, T., Deschamps, C. J., Rodrigues, T. T. (2017). A New Modeling Strategy to Simulate the Compression Cycle of Reciprocating Compressors. Proceedings of the 9th International Conference on Compressors and Coolants (Paper 226). Bratislava, Slovakia.